Original article

A switchable sensor for Cu^{2+} and Zn^{2+} based on xanthene moiety-making a path for a complex molecular encryption system based on color and fluorescent change

Amar Raj[a], Ankur Gupta[a]*

[a]*Department of Chemistry, Indian Institute of Science Education and Research Bhopal, Bhopal Bypass Road, Bhauri, Bhopal 462066, Madhya Pradesh, India. E-mail: ankurg@iiserb.ac.in.

Abstract: Colorimetric and fluorescent detection methods for metal analytes has become a powerful tool for qualitative and quantitative analysis in the last decade due to their immediate output, cost-effectiveness, specificity/selectivity, zero interference, high detection limit, and application in practical samples. Sensing Cu^{2+}, $Ni^{2+,}$ or Zn^{2+} like analytes gained a lot of attention due to their significance in biological, medical, and environmental purposes. To account for this purpose, we synthesized and designed a colorimetric, fluorescent off-on, and reversible chemosensor **EYM** having xanthene as a signaling moiety and 4-carbamoyl-3-Butenoic acid as a receptor moiety. The **EYM** probe is then screened with Al^{3+}, V^{3+}, Na^{+}, K^{+}, Fe^{3+}, Mg^{2+}, Ca^{2+}, Fe^{2+}, Co^{2+}, Zn^{2+}, Cd^{2+}, Hg^{2+}, Mn^{2+}, Co^{3+}, Pb^{2+}, Cu^{2+}, Pd^{2+}, and V^{4+} in DMSO: H_2O (4:1) solvent system where **EYM** shows absorbance change specifically for Cu^{2+} at 541nm changing from colorless to dark pink. The detection limit and association constant of the **EYM** probe for Cu^{2+} is 78.5nM and (6.013-5.947)×10^9 $M^{-1,}$ respectively. The coordination of Cu^{2+} with **EYM** is in (1:2: Ligand: Metal) stoichiometric ratio. The immediate saturation time (~2 sec) and low detection limit (78.5nM) of the EYH probe give competitiveness over other sensors in practical applicability in real-life samples detection of Cu^{2+}. Not only this, the **EYM** sensor can switch from mono to bi to tri-functional sensor for Cu^{2+}, $Ni^{2+,}$ and Zn^{2+} with the stimuli of water in the DMSO solvent. The **EYM** shows specific abnormal fluorescent enhancement in contact with Zn^{2+} in DMSO solvent. The detection limit for Zn^{2+} is 79nM same as Cu^{2+} in a colorimetric assay. Switchable sensing is utilized to make complex molecular LOGIC GATE operations, including password-protected molecular encryption systems.

Keywords: Inter charge transfer (ICT); Eosin Y; Chemosensor; Benesi-Hildebrand plot (BH plot); Quencher EDTA (Ethylenediaminetetraacetic acid); Molecular logic gate; Encryption

1. Introduction

The development of chemical probes for metal analytes has gained significant attention due to its potential application for environmental, medicinal, biological, and chemical purposes. Chemosensors have a receptor unit containing a binding pocket for metal cations, anions, or molecules. These binding pockets have coordinating atoms like N, O, S, which facilitate coordinating metal cations like Cu^{2+}, Ni^{2+}, and $Zn2^{+}$.[1–7] The binding of analytes brings a physical and chemical change in the overall system, resulting in a rise in the signal detected by optical probes. Czarnik and coworkers were among the first who utilized the close and open ring feature of rhodamine B hydrazide as a sensor for Cu^{2+}.[8] Rhodamine hydrazide contains a signaling core as a xanthene unit and receptor site as a hydrazine carboxaldehyde moiety. On binding with an analyte, the spiro ring breaks to fuel up the xanthene core with aromaticity, resulting in a rise of fluorescence and absorbance signal. Developing chemosensor also plays a vital role in qualitative and quantitative analysis of metal ions "in the field." Several methods have been used to detect metal ions, such as atomic absorption spectroscopy,[9] inductively coupled plasma-mass spectrometry,[10] inductively coupled plasma emission spectroscopy,[11] neutron activation analysis,[12], etc. Still, it is not suitable for "in the field" detection due to critical pretreatment procedures, time-consuming analysis, expensive instruments, and often has serious interference by co-existing ions. But the chemosensor with fast response time, selective and low LOD (Limit of Detection) can play an important role "in the field" detection.

Copper is one of the ubiquitous and essential minerals that play a more significant role in day-to-day human activities in biological systems. Many natural enzymes, organelles, and metabolism are dependent on Cu^{2+} for working in healthy mode.[13,14] The benefits of copper to human life come with an apparent condition: the controlled intake of copper. The US Environmental Protection Agency (EPA) has set the maximum allowable level of copper in drinking water at 1.3 ppm.[15] Excess and deficiency of copper can lead to oxidative stress, damage to the kidney and liver, to life-threatening neurological disorders like Alzheimer's, Wilson's, and Menke's diseases.[16–22]

Zinc is the second most abundant transition metal in the human body. Chemosensor based on zinc has attracted significant attention due to its high relevance in a biological system as Zn^{2+} is one of the most essential cations in catalytic centers and structural cofactors of many Zn^{2+}-containing enzymes and DNA-binding proteins (e.g., transcriptions factors).[23] Zinc is believed to be a vital factor for many biological processes such as brain function and pathology, gene transcription, immune function, and mammalian reproduction, as well as some pathological processes, such as Alzheimer's disease, epilepsy, ischemic stroke, and infantile diarrhea.[24–26] Zn^{2+} has a d^{10} configuration, a spectroscopically silent cation that was extensively studied via fluorescent chemosensor.[27–30]

Nickel is a reasonably toxic element in the biological system.[31] Nickel is also an essential element because of its usage as the catalyst and in batteries, electroplating, welding, ceramics, paint pigments, dental prostheses, and magnetic tapes.[32] Deficiency and excess nickel can result in severe health deterioration. It can cause nickel-eczema, cancer of the respiratory system, acute pneumonitis, asthma, and an increase in blood cells.[33,34] It can effects badly on blood, kidney, respiratory, and central nervous systems.[35,36] Thus, these metal analytes have been the primary targets of chemosensor researchers because of their harmful effects on the ecosystem and the human body. [37–40]

Here we have designed a chemosensor based on Eosin Y. The xanthene unit acts as a signaling unit while 4-carbamoyl-3-Butenoic acid as a receptor moiety that can sense Cu^{2+}, Ni^{2+}, Zn^{2+} in optimized condition. Eosin dye has been extensively used for differential staining of connective tissue and cytoplasm and stains in pink-orange color –well known in histology.[41,42] Eosin Y absorbs green light and shows a characteristic peak at 532nm in UV-Visible absorption spectroscopy with a molar extinction coefficient of 1.10×10^5 $M^{-1}cm^{-1}$.[43,44] Eosin Y had been applied in various visible light photocatalysts in organic syntheses such as reductive dehalogenation, desulfonylation, and deoxygenation, oxidation of benzyl alcohol, carbonylation of arene diazonium salt, and many others.[45–52] Eosin Y-based chemosensor will add a wing to its enormous applicability in the chemical and biological samples.

Our work in this area has focused on optical methods and has explored a chemosensor system (EYH) based on the concept of intramolecular charge transfer (ICT). In this work, we report the design and synthesis of a novel eosin-based chemosensor (**EYM**) through the reaction of Eosin hydrazide and maleic anhydride for the detection of metal ions in aqueous media. In this respect, the **EYM** was investigated and observed to exhibit highly selective colorimetric and fluorescence sensing abilities for Cu^{2+} and Zn^{2+}, respectively. The optical properties were investigated using UV-Vis and fluorescence analyses in organic solvent and aqueous media to determine the colorimetric response of **EYM** for Cu^{2+} for various applications, such as molecular encryption system, paper and silica-based sensor, and recovery of analyte in practical samples.

2. Experimental section

2.1. Synthesis of EYH

The Eosin hydrazide was synthesized from parent molecule Eosin Y via condensation reaction with hydrazine. The hydrazine was taken in hydrazine hydrate (NH_2-NH_2. H_2O) form and used in the reaction in specific conditions (solvent: Dichloromethane (DCM) or Chloroform ($CHCl_3$); Reflux at 40^oC for DCM and 60^oC for chloroform). 100mg of Eosin Y (molecular weight: 691.85gm/mol) was taken in a round bottom flask. An excess of hydrazine hydrate (molecular weight: 50.06gm/mol, 20 equivalence, 140uL) was slowly added to the reaction mixture containing 5mL of solvent. The resultant mixture was then left out overnight with continuous stirring and refluxing. A white precipitate would form after keeping overnight which would be clearly visible by the naked eye. The resultant precipitate was washed thoroughly with 100mL of water and allowed to dry in the oven completely. The resulting white precipitate was weighed and found to be a 68.5% (65 mg) yield. The structure was characterized by ^{1}H-NMR, ^{13}C NMR, and ESI mass spectra **Figure S11, S12, S13**.

2.2. Synthesis of EYM

The **EYM** was synthesized using EYH and Maleic anhydride **Scheme 1**. First, maleic anhydride (21mg, 2 equiv) was solubilized in DCM then slowly added to the reaction mixture, which contains EYH (70mg) in DCM (5ml) solvent. The addition was done while stirring. After the completion of mixing, 1% DMF was added and allowed to reflux overnight. The resultant mixture was washed and recrystallized with cold methanol. The yield of the final product (**EYM**) was 24mg

(29.86%). 1H NMR, Mass spectrometry, characterized the compound **Figure S1, S2**.

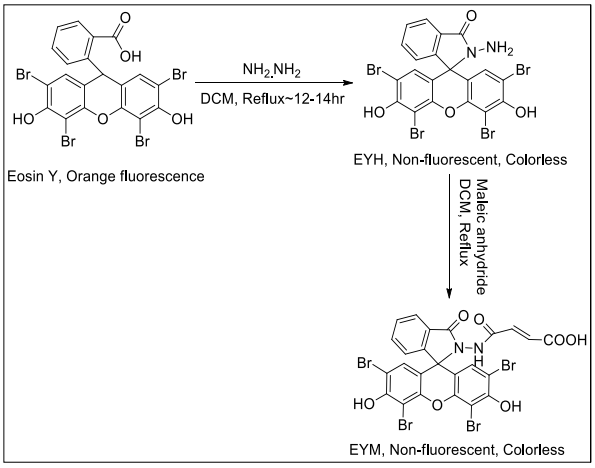

Scheme 1: Synthetic procedure of **EYM**.

2.3. Time-resolved fluorescence measurement

Fluorescence lifetime or time-resolved fluorescence measurement was carried out using time-correlated single-photon counting (TCSPC) setup from a Hamamatsu MCP photomultiplier (R2 3809U-50). The 509 nm pico-second laser was used as an excitation source for the lifetime measurements. The photon count was set up to 10,000. The instrument response function (IRF) was measured using a dilute suspension of Ludox (Sigma Aldrich) before starting the measurement. The emission polarizer was fixed at a magic angle (54.7^o) with respect to the excitation polarizer. The bi-exponential decay was determined by using the deconvolution method in supplied software DAS v6.2. The fitting parameter (chi-square value (χ^2)) is considered in the range from 0.9-1.2. Lifetime measurement by TCSPC was performed at room temperature (298 K). The fitting was done by using formula $N(t) = C_o+N_o\, e^{-t/\Gamma}$ (monoexponential function for free $CuSO_4$, **EYM**) while for **EYM**+Cu^{2+} biexponential function was used where the fitting formula was $[N(t) = C_o+N_1\, e^{-t/\Gamma_1} +N_2\, e^{-t/\Gamma_2}]$ which then averaged out for calculating the lifetime.

2.4. Analytical procedure and Calculations

The stock solution of **EYM** was prepared in DMSO solvent while the metal analytes stock solution of 10mM was prepared in Water-Ethanol solvent. For colorimetric measurements, the volume inside the quartz cuvette (1 cm path length) was fixed at 800uL, while for fluorometric measurements, the volume inside the quartz cuvette (1 cm pathlength) was set at 2mL. The association constant was calculated using the modified Benesi-Hilderbrand equation.

$$L + nCu^{2+} \underset{}{\overset{k}{\rightleftharpoons}} L(Cu^{2+})n$$

$$\frac{A-A_{min}}{A_{max-}A} = \frac{[LCu^{2+}]_n}{[[LCu^{2+}]_{n_{max}}-[LCu^{2+}]_n]} = \frac{[LCu^{2+}]_n}{[Lo-[LCu^{2+}]_n]} = k[(Cu^{2+})_o]^n \quad \ldots\ldots\ldots\ldots (1)$$

A_{min} is the absorbance of the probe without analyte, A_{max} is the absorbance of a probe in the presence of an excess of analyte and while A is the absorbance of probe in presence of Cu^{2+} analyte. In the presence of excess of Cu^{2+} analyte $[LCu^{2+}]_{n_{max}}$ is almost equal to L_o. Using this approximation in **equation 1**:

$$\frac{A-A_{min}}{A_{max-}A} = K[(Cu^{2+})_o]^n \quad \ldots\ldots\ldots\ldots\ldots\ldots\ldots\ldots (2)$$

$$\log\frac{A-A_{min}}{A_{max-}A} = \log\{K[(Cu^{2+})_o]^n\} \quad \ldots\ldots\ldots\ldots\ldots\ldots (3)$$

$$\log\frac{A-A_{min}}{A_{max-}A} = \log(k) + n\log[(Cu^{2+})_o] \ldots\ldots\ldots\ldots\ldots (4)$$

For 1:2 stochiometry where n=2, the equation obtained:

$$\log\frac{A-A_{min}}{A_{max-}A} = \log(k) + 2.\log[(Cu^{2+})_o] \ldots\ldots\ldots\ldots\ldots (5)$$

Or in linear form (Here, n=2),

$$\frac{1}{(A-Ao)} = \frac{1}{\{K(Amax-Ao)\,[Cu^{2+}]2\}} + \frac{1}{[Amax-Ao]} \ldots\ldots\ldots (6)$$

Equation 6 is further used to predict the association constant for the 1:2 stochiometry binding model.

The Limit of Detection was calculated using the formula $\frac{3\sigma}{k}$ where σ (sigma) is the standard deviation of the blank sample while k is the calibration plot slope.

2.5. Procedure for paper and silica-based sensor

Analytes $CuSO_4$ and $ZnSO_4$ were dissolved in methanol to make a 1mM solution in which filter papers were incubated for 2 minutes. After incubation, these papers were dried in an oven for 2 minutes, which gives the inoculated papers. The resultant paper was inked with **EYM** solution. The resulting papers were allowed to dry in the air for 1 minute to observe the color change. For the silica gel-based sensor, silica plates were incubated in the above analyte solution. The resultant plates were dried in air for 5 minutes and then allowed to ink with 1mM solution of EYH. The plates were allowed to dry in the oven for 5 minutes to observe fluorescent and color change.

3. Result and discussions

3.1. Coloromteric sensing of EYM

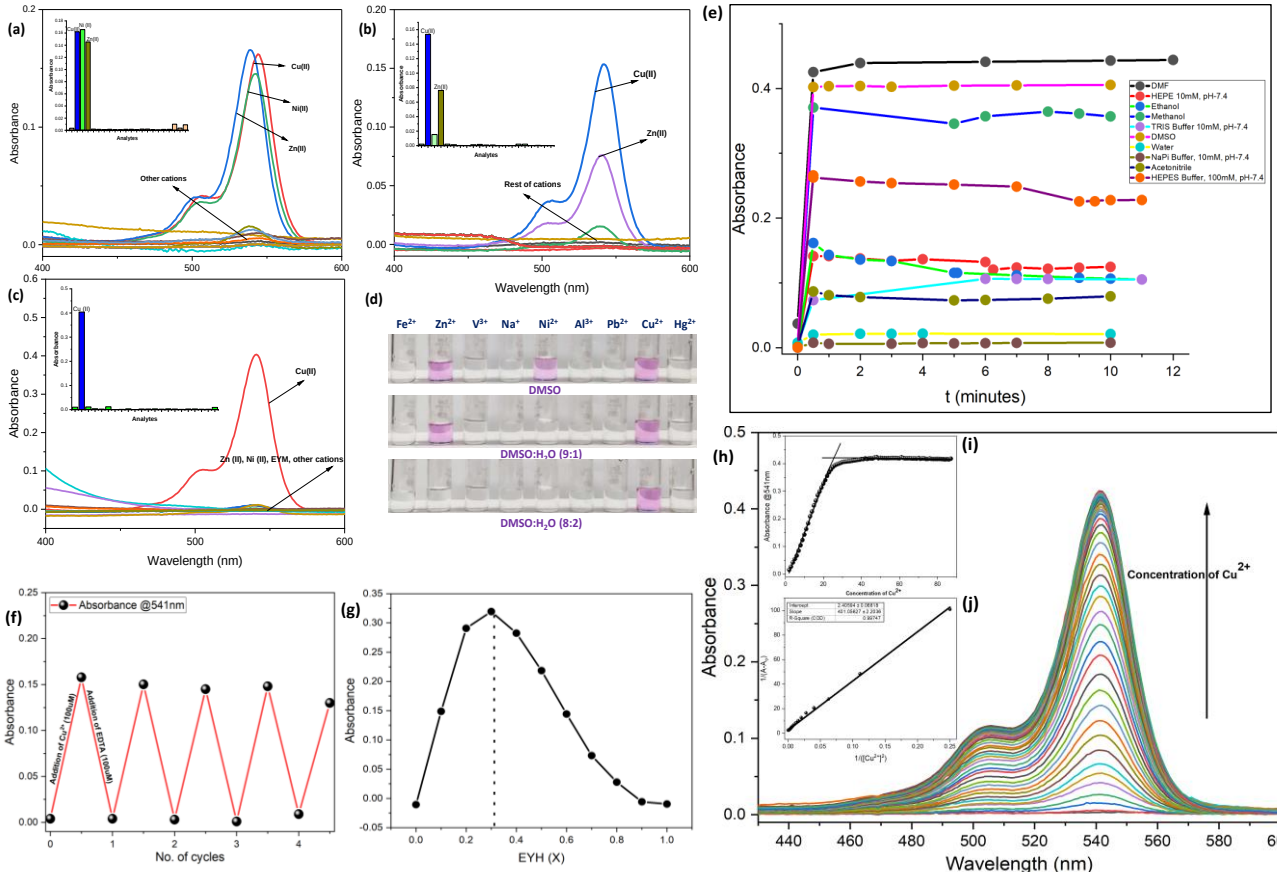

Figure 1: (a) Absorbance response for **EYM** (2uM) in the presence of analytes of 100uM in DMSO solvent. **(b)** Absorbance response for **EYM** (2uM) in the presence of analytes of 100uM in DMSO: H_2O (9:1) solvent. **(c)** Absorbance response in spectral form for **EYM** (5uM) in the presence of analytes of 100uM. Only Cu^{2+} shows a significant absorbance signal in solvent system DMSO.H_2O (8:2). **(d)** Real pictures of vials having analytes (Fe^{2+}, Zn^{2+}, V^{3+}, Na^{+}, Al^{3+}, Cu^{2+}, Hg^{2+}) and **EYM** in solvent system given in (a), (b), and (c). **(e)** Absorption response of **EYM** in the presence of copper where time is the variable entity. The concentration of **EYM** was 5uM, and Cu^{2+} was 200uM. The individual point is the highest peak of absorbance signal from its spectra. **(f)** Effect of EDTA (quencher) on absorbance signal response by **EYM** in the presence of Cu^{2+}. The concentration of **EYM** was taken as 2uM and concentration of Cu^{2+} and EDTA was 100uM. The reversibility cycle was successfully repeated 4 times in solvent system DMSO: H_2O (8:2). **(g)** Job's method analysis for **EYM**- Cu^{2+} complexation. The total concentration was fixed at 20uM in solvent system DMSO: H_2O (8:2). **(h)** Absorbance spectra for **EYM** (5uM) in the presence of Cu^{2+} in solvent system DMSO.H_2O (8:2). The Cu^{2+} concentration varies from 0uM to 87uM. **(i)** Linear and saturation plot for the absorbance at respective λ_{max}. **(j)** Plot between 1/ (A-Ao) and $1/[Cu^{2+}]^2$ fitted with the linear relationship of Benesi-Hildebrand equation.

EYM was synthesized using the addition of maleic anhydride with Eosin hydrazine. The **EYM** is a non-fluorescent compound and has no absorption in the visible region. Density functional theory (DFT) calculations were employed to elucidate the most stable form of **EYM**. The HUMO-LUMO molecular orbital shows a clear shift of electron density from xanthene unit (HOMO) to 4-carbamoyl-3-Butenoic acid moiety (LUMO) **Table S1**. The HOMO-LUMO gap was calculated to 3.90eV, which corresponds to a 320nm absorbance peak in the UV-Vis spectroscopy **Figure S3**. The colorimetric response of probe **EYM** was studied based on solvent-solute interaction. It has been already known that solvent plays a critical role in chemosensor coordination with analytes due to solubility, dipole alignment, and other factors. To study the effect on the interaction of **EYM** with Cu^{2+}, we chose a series of organic solvent and aqueous buffers that are DMF, DMSO, Acetonitrile, Ethanol, Water, Methanol, HEPES Buffer (10mM pH-7.4; 100mM pH-7.4), NaPi Buffer (10mM, pH-7.4), and TRIS Buffer (10mM, pH-7.4). It was found that the solubility factor in organic solvents dominates the behavior of **EYM** since the absorbance intensity is highest in DMF and DMSO **Figure 1e**. The **EYM** is highly soluble in DMSO and DMF, which may facilitate the coordination of Cu^{2+} binding with **EYM**, which results in the opening of the spirolacatam ring. In buffers, HEPES (100mM, pH-7.4) shows the highest absorbance increment, which is comparable to DMSO and DMF solvent.

Since HEPES contains coordinating atoms O, N, and S, which may have facilitated the **EYM**-Cu^{2+} complexation. The saturation time of complexation in DMSO is ~1-2 sec, which gives a significant advantage over other Cu^{2+} based colorimetric sensors. Thus, the DMSO reaction system was chosen for further study via colorimetric assay of **EYM**.

Specificity or selectivity is a major application for the chemosensor and in its development. In pursuance of qualitative and quantitative analyte analysis in real-life samples by probe **EYM**, it needs to give a specific response to a particular analyte. To study the **EYM** behavior in complexation, we take the DMSO solvent system and screen with 18 different analytes-Al^{3+}, V^{3+}, Na^{+}, K^{+}, Fe^{3+}, Mg^{2+}, Ca^{2+}, Fe^{2+}, Co^{2+}, Zn^{2+}, Cd^{2+}, Hg^{2+}, Mn^{2+}, Co^{3+}, Pb^{2+}, Cu^{2+}, Pd^{2+}, and V^{4+}. In DMSO (100%) solvent, **EYM** gives colorimetric response to three analytes Cu^{2+}, Zn^{2+}, and Ni^{2+}, while it shows no response to other analytes **Figure 1a**. The absorbance intensity for three analytes has a similar value for **EYM** (2uM), while the analyte's concentration is 100uM. The DMSO system's result shows **EYM** as multifunctional sensor, but it changes its specificity toward analytes in the presence of co-solvent. Here we induce H_2O as a co-solvent in the DMSO reaction system in 9:1 v/v % proportion, the absorbance intensity of Ni^{2+} diminishes significantly while the Cu^{2+} signal does not change at all **Figure 1b**. Now the significant absorbance intensity comes from Cu^{2+} and Zn^{2+} while for others, the absorbance intensity is negligible to none, making **EYM** a bi-functional sensor for Cu^{2+} and Zn^{2+}. For solvent system (8:2 v/v %) of DMSO: H_2O, we achieve the specificity for Cu^{2+}, showing abnormal absorbance enhancement **Figure 1c** due to complexation while it shows no signal for other analytes for **EYM** (5uM) in the presence of 100uM of analytes **Figure 1d**.

To establish if the chemosensor has a reversible or non-reversible binding with Cu^{2+}, we use a strong chelator for quenching Cu^{2+} from the reaction system. The experiment was carried out with **EYM** (2uM) in the presence of 100uM of Cu^{2+}, and 100uM EDTA was added alternatively to observe the increment and decrement of absorbance intensity. **Figure 1f** clearly showed the ~100% reversibility and was able to carry out at least 4 cycles with close to complete reversibility. The absorbance signal's on-off can only be explained by the fact that $EDTA^{2-}$ de metallates the Cu^{2+} ions from **EYM**-Cu^{2+} solutions. Thus it ticks the reversibility criteria to be the ideal receptor for Cu^{2+}. The inference study was done in solvent system DMSO: H_2O (4:1) with **EYM** of 4uM and analytes of concentration 40uM. Among all the analytes, Al^{3+} shows a significant interference by quenching the absorption response of **EYM** **Figure 2**. The same analyte was also confirmed to show interference in Hepes buffer (ph-7.4, 100mM) but with less impact on response signal **Figure S6**.

To understand the binding mechanism, one of the prerequisites is to know the binding stoichiometric ratio. For this purpose, we perform the Job's analysis with **EYM** and Cu^{2+} in solvent system DMSO: H_2O (4:1), where the total concentration was fixed at 20uM. The result showed in **Figure 1g** shows a clear picture of the 1:2 (Ligand: Metal) binding ratio. Multiple metal-binding site presence may be the reason for immediate detection or less saturation time. Based on the 1:2 binding stoichiometry model, the association constant and Limit of Detection were calculated using the Benesi-Hildebrand equation and $3\sigma/k$, respectively. The association constant of **EYM**- Cu^{2+} in DMSO: H_2O (4:1 v/v %) solvent system was calculated to be **$(6.01\text{-}5.95)\times 10^{9}$ M^{-1} Figure 1h, 1i, 1j** and in HEPES buffer, 100mM, pH-7.4 it was calculated to be **$(2.96\text{-}3.05)\times 10^{9}$ M^{-1} Figure S4, S5.** The detection limit was estimated to be 78.5nM and 1.73uM for DMSO: H_2O (4:1) and HEPES Buffer, respectively. The high association constant is concurrent with the fact of the presence of multiple sites. The Limit of Detection also suggests that it can detect the sub-micromolar concentration of Cu^{2+} in practical samples.

Since rhodamine and coumarin-based chemosensor had been reported as a pH sensor combined with a sensor for analytes as chemosensor itself, it loses its integrity in acidic or basic pH. To study the response of **EYM** in the presence of variable H^{+}/OH^{-} concentration, the absorbance intensity was monitored w.r.to different pH scales in two different samples: **EYM** (2uM) in the absence of analyte and **EYM** (2uM) in the presence of Cu^{2+} (100uM). The pH scale was varied from 1.25 to 12.36 pH using HEPES solution (100mM): DMSO (9:1). As shown in **Figure 3**, **EYM** is stable throughout the entire pH range, while **EYM** complexation with Cu^{2+} was seen in 5-9 pH range while it shows negligible absorbance signal beyond this pH pocket. The maxima of absorbance signal ~7-8 pH unit range. Thus, pH 7.4 was chosen to study **EYM** complexation in an aqueous buffer.

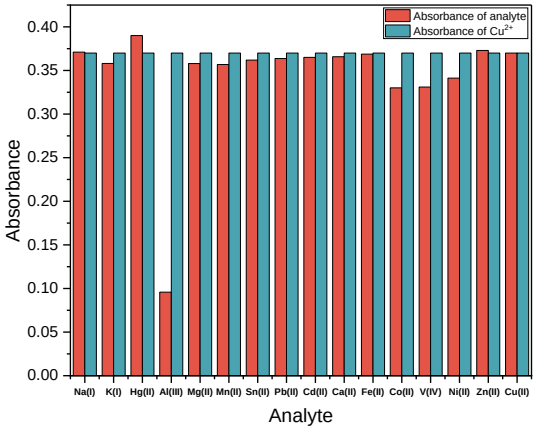

Figure 2: Absorption response of **EYM** (4uM) in the presence of Cu^{2+} (40uM) and analytes (40uM) in solvent system DMSO: H2O (4:1v/v).

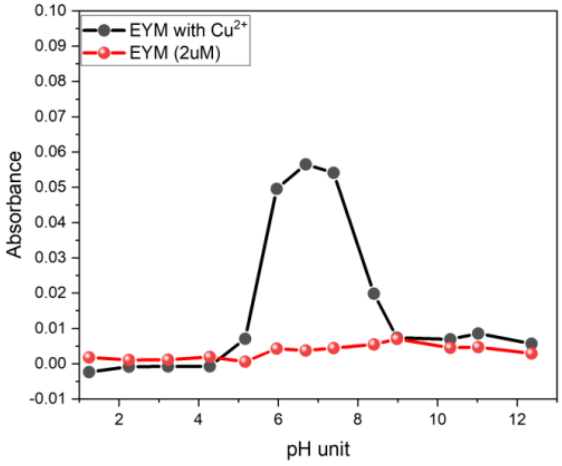

Figure 3: Effect of pH on **EYM** complexation with copper. The solution used here was HEPES (100mM): DMSO (9:1). The concentration of **EYM** is 2uM, and the concentration of Cu^{2+} is 100uM.

3.2. Fluorescence response of EYM

The **EYM** has been optimized for colorimetric assay, where it has shown the specificity of Cu^{2+} in DMSO with co-solvent water. It also showed a rare conversion of a mono-bi-tri functional sensor for Zn^{2+} and $Ni^{2+,}$ which indicates the potential usage of **EYM** in diverse conditions. To study the fluorescence response of **EYM**, we screen **EYM** with different analytes and record the fluorescence response in DMSO solvent, as shown in **Figure 4a**. It clearly shows the abnormal enhancement specific for Zn^{2+} in all 18 analytes. For Cu^{2+} and Ni^{2+}, **EYM** does not show any change in response signal, which may be due to its paramagnetic nature. The reversibility was also checked for the **EYM**-Zn^{2+} complexation upon adding EDTA **Figure 4c**. We were able to complete 3 cycles with almost 100% absorbance recovery. The Job's analysis shows the 1:2 stochiometric binding between **EYM** and Zn^{2+} **Figure 4b**. We estimated the association constant and detection limit via fluorescence titration of **EYM** with Zn^{2+}. Association constant was calculated to be $(2.25\text{-}2.29)\times10^{8}M^{-1}$ while the measured detection limit was 79nM for **EYM**-Zn^{2+} in DMSO solvent **Figure 4d, 4e, 4f**. We had analyzed the specificity of **EYM** towards Zn^{2+}, but the question is whether Cu^{2+} shows

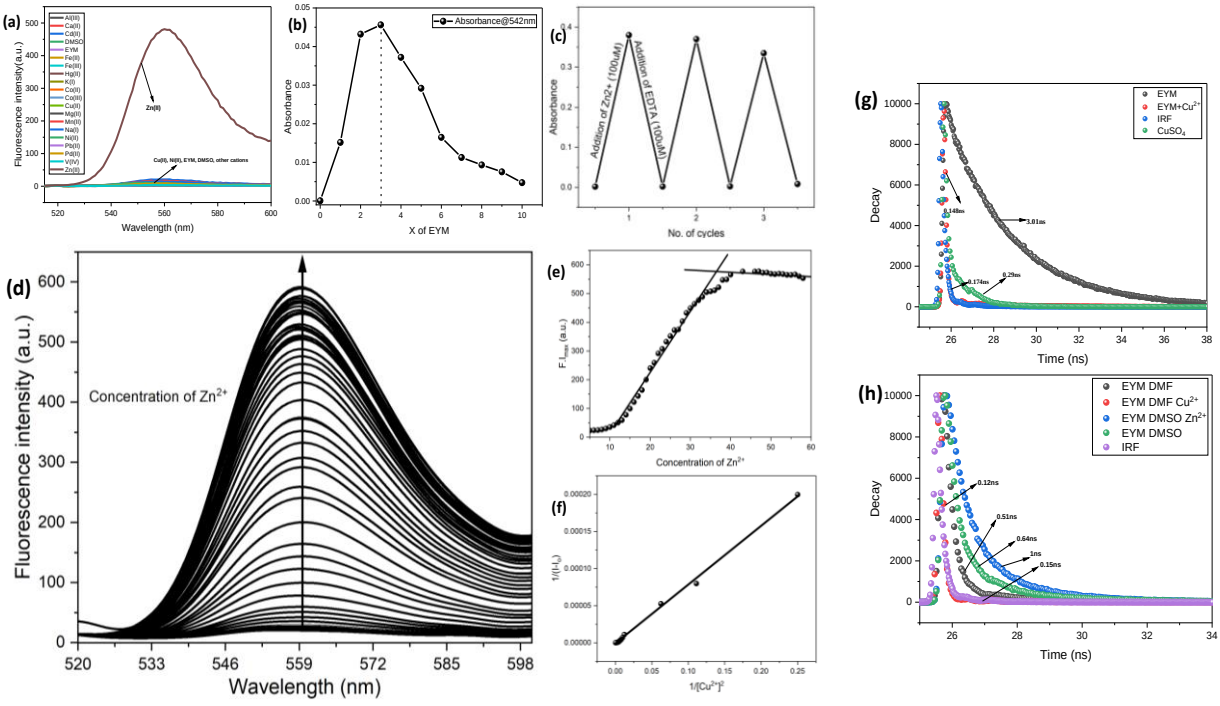

Figure 4: (a) Fluorescence response in spectral form for **EYM** (1uM) in the presence of analytes of 100uM. The solvent chosen for the experiment was DMSO. **(b)** Job's method analysis for **EYM**- Zn^{2+} complexation in DMSO solvent system. The total concentration was fixed at 20uM. **(c)** Reversibility of **EYM**-Zn^{2+} complexation on addition of cheletor EDTA. The conacentration of **EYM** is 5uM and 100uM of Zn^{2+} and EDTA. **(d)** Fluorescence signal response of **EYM** (1uM) in the presence of varying Zn^{2+} concentration (1 to 63uM) **(e)** Linear and saturation curve plot of titration using λ_{max} at 550nm. **(f)** Benesi-Hilderbrand plot using 1/(I-Io) vs. $1/[Zu^{2+}]^2$ as y and x-axis. The solvent taken here was DMSO. **(g)** The fluorescence lifetime plot for **EYM** in the presence and absence of excess Cu (II), free Cu (II) in the form of Copper sulfate salt, and IRF (Instrument Response Function) in solvent system DMSO: H_2O (8:2). **(h)** The fluorescence lifetime plot for **EYM** in the presence and absence of excess Cu^{2+} in DMF solvent, **EYM** in presence and absence of Zn^{2+} in DMSO solvent.

fluorescence enhancement or quenching with respect to solvent. This study's parameter is the F/Fo value; here, F belongs to the fluorescence intensity of **EYM** in the presence of Cu^{2+}, while Fo is the value of **EYM** in the absence of Cu^{2+}. The solvent chosen for this purpose is a mixture of organic solvents and an aqueous buffer. **Table S2** suggests that solvent plays a major role as Cu^{2+} shows strong paramagnetic quenching in DMF, while it shows fluorescence enhancement in methanol and ethanol. The parameter F/Fo may only give the relative comparison, but to observe the propensity of quenching and enhancement, we should compare the $F.I_{max}$. In **Figure S7**, the quenching in DMF solvent is much intense than any other turn-on or turn-off in solvents. This observation indicates that the non-fluorescence **EYM** changes to fluorescence state in DMF solvent by spiro ring opening. After coordination of Cu^{2+} with receptor site, the paramagnetic quenching takes place, resulting in a decrement in fluroscence signal while no absorbance change was recorded. Thus **EYM** can act as a sensor for DMF solvent via fluorescence enhancement.

3.3. Lifetime studies of EYM sensing

To understand the mechanism and effect of analyte's presence in **EYM** solution, we measured the lifetime of EYM in the presence and absence of analyte. First, we analyze the findings of **EYM** for colorimetric assay, which suggests **EYM** shows turn-on for Cu^{2+} in DMSO: H_2O (4:1) solvent, but fluorescence study tells us that there is no significant enhancement in the above solvent. The findings from lifetime spectra reveal the same as **EYM** has 3 ns lifetime while adding the excess Cu^{2+} in DMSO: H2O (4:1) solvent the lifetime significantly reduces to 0.15 ns **Figure 4g, S8**. After opening the spirolactam ring, the new compound form shows no fluorescence on interaction with Cu^{2+} due to its paramagnetic quenching. The fluorescence study also tells us that there is a change in the structural property of **EYM** in DMF solvent and has fluorescence quenching upon interaction with Cu^{2+}. In **Figure 4h, S9, EYM** has a lifetime of 0.51ns. In contrast, this lifetime shows significant decrement upon addition of Cu^{2+} to 0.12 ns which suggests that there is indeed fluorescence quenching.

As **EYM** has been found to show specific abnormal fluorescence increment in the presence of Zn^{2+} in DMSO solvent, this finding should be concurrent with lifetime measurement. From **Figure 4h**, the **EYM** shows 0.64 ns in the DMSO solvent system, while the addition of excess Zn2+ increases the lifetime to 1ns, indicating the formation of a high fluorescence compound. The above result is consistent with the spirolactam ring-opening in **EYM** on coordination with Zn^{2+} and paramagnetic quenching of Cu^{2+}.

4. Binding mechanism of EYM

The binding mechanism for **EYM** in the presence of Cu^{2+} was studied. As already discussed, Job's plot analysis gives a 1:2 binding ratio between host and guest in DMSO-H_2O (4:1) solvent system. The color reaction of **EYM** with Cu^{2+} is attributed to the ring-opening of the spirolactam structure promoted by Cu^{2+} complexation. However, the reaction system hardly shows any fluorescence. Considering all, the color response of **EYM** with Cu^{2+} can be explained via **scheme 2**. The hydrazide and carboxyl groups in **EYM** produce a cooperation effect, leading to the 1:2 complex formations. The two Cu^{2+} ions in the complex may play a very different role: one induces the opening of the spirolactam structure, and the other quenches the fluorescence of the xanthene moiety. The binding of Cu^{2+} was studied with the help of FT-IR spectroscopy. Upon addition of Cu^{2+} in **EYM** solution, the $1663cm^{-1}$ band shifted to $1645cm^{-1,}$ which corresponds to C=O groups, while the $1023cm^{-1}$ band shifted to $1010cm^{-1,}$ which corresponds to C-N group **Figure 5**. The shift to the lower wavelength is due to a decrement in electron density which suggests that the functional group participates in coordination with Cu^{2+}.

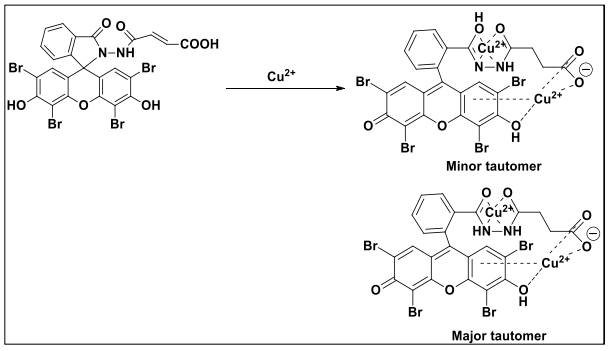

Scheme 2: Binding mechanism of Cu^{2+} with **EYM** according to 1:2 stoichiometric ratios.

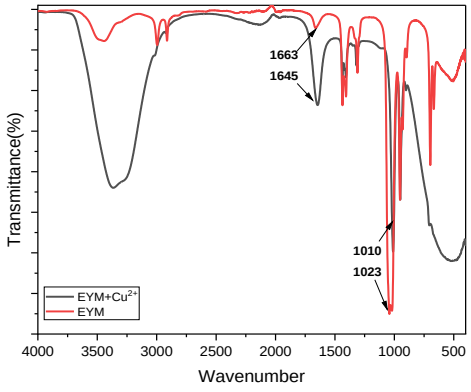

Figure 5: Binding study using FT-IR spectroscopy of **EYM** in presence and absence of Cu^{2+} using (ATR) as an additional accessory unit. In IR, black color belongs to the complex of EYH with Cu^{2+} while red color belongs to EYH in the absence of Cu^{2+}.

5. Application of EYM

5.1. Application in practical samples

To test the applicability in practical samples, the **EYM** sensor was applied to drinking water sample **Figure S10A** and buffered human serum albumin samples **Figure S10C** as it has been reported that Cu^{2+} ions in human blood are found to be bounded with mainly two proteins: human serum albumin (HSA) and ceruloplasmin (CP).[53–56] Further, it was applied in industrially made sanitizer with Cu^{2+} spiked concentration to recognize its industrial needs **Figure S10B**. The above Cu^{2+} spiked samples' concentration was analyzed by the proposed method using the calibration plot in Type 1 water under optimized conditions. The samples were prepared using DMSO as co-solvent for drinking water and industrial product sample, while the BHSA sample was prepared in Hepes buffer (100mM, pH-7.4). The recovery percentage was found to be in range of (90-103) % for drinking water and industrialized product samples, while the recovery percentage was (101-122) % for BHSA samples, indicating the interaction of Cu^{2+} with HAS **Table 1**. To further study we observe the absorption response with varying concentrations of HSA in solution mixture having an excess of Cu^{2+}. We found a decrement in absorbance signal as the concentration of HSA increases but it became steady for a higher concentration of HSA **Figure S10D**. This shows that the concentration of HSA affects the kinetics of **EYM**-Cu^{2+} complexation but doesn't show abnormal increment/decrement in absorbance signal.

5.2. Application in molecular logic gates

Simple molecular Boolean logic gates can be integrated to obtain more complicated combinational molecular gates, allowing a single molecule to process complex operations. Utilizing previous observations, **EYM** can form a complex and efficient logic gate as it can switch sensitivity based on solvent. Thus, we designed a molecular-logic gate where the inputs include Zn^{2+}, Cu^{2+}, Ni^{2+}, DMSO and H2O and output is a simple color on/off.

In **Figure 6a**, we first designed logic gate for analyte Cu^{2+} which give rise in absorbance intensity in all three different solvent system. With input 1 for Cu^{2+}, the output should be color on (1) in (DMSO; DMSO-H_2O 8:2; DMSO-H_2O 9:1) while for Ni^{2+} with input 1, the output 1 should be in Color ON (DMSO) while it should give output 0 for other two solvents **Figure 6b**. Similarly, with analyte Zn^{2+} input 1 should have output 1 in two solvents (DMSO, DMSO-H_2O 9:1) while it should give 0 output in DMSO: H_2O (8:2) **Figure 6c**. To satisfy these condition we use a combination of AND, OR and NOT gate. By running Zn^{2+} and Ni^{2+} in negative logic mode and combining with Cu^{2+} in AND gate we create a positive output specifically for Cu^{2+} in DMSO:H_2O (8:2) solvent system. Same method we use to create a positive logic mode for Cu^{2+} and Zn^{2+} by putting Ni^{2+} in negative mode and combining individual gate by AND gate to give output-color on. Previous observation suggests that the **EYM** shows a fluorescent turn-on sensor for Zn^{2+} while there is no change in fluorescence in Ni^{2+} and Cu^{2+} in DMSO solvent system. To develop password-protected molecular encryption we employed four input modes include Ni^{2+}, Cu^{2+}, Zn^{2+}, and DMSO, where positive results only come from input 1 for DMSO and Zn^{2+} while any other combination will give the negative output. As shown in **Figure 6f, 6g**, the combination 1101 does not give any output while 0011 gives the positive output. There can be 16 combinations of binary code and one holds true, which can be potentially used as a molecular encryption system.

5.3. Application in paper and silica-based sensor

To investigate the further potential application of designed sensor EYH, paper and silica-based strips were prepared for rapid in-field and on-spot detection of Cu^{2+} and Zn^{2+} analyte. For this purpose, 1mM of analyte was incorporated into filter papers using DMSO as solvent. The resultant inoculated paper was allowed to dry in the oven and then applied with **EYM** concentration of 1mM. As speculated, an apparent visible color change from colorless to pink appeared immediately in few seconds. For Zn^{2+}, the color change was accompanied with orange fluorescence **Figure 6e**. Furthermore, the **EYM** was also employed with a silica-based strip performed via the same upper method. A significant visible color change was seen immediately by the naked eye, while a substantial fluorescence change can be seen under UV light **Figure 6d**. The intensity of color can be potentially employed to know the concentration of Cu^{2+} or Zn^{2+}.

Sample	Cu^{2+} spiked (uM)	Cu^{2+} recovered(uM)	RSD (n=3)
Buffered Serum albumin[A]	2	2.02(101.2%)	0.5%
	5	6.12(122.5%)	2.1%
	40	45.08(112.7%)	6.2%
	60	64.86(108.1%)	2.1%
Drinking Water[B]	2	2.07(103.5%)	1.2%
	5	4.67(93.5%)	0.8%
	10	9.31(93.1%)	2.1%
Industrial sanitizer[C]	2	1.78(89.1%)	0.6%
	5	4.51(90.2%)	0.3%
	10	10.2(102%)	0.2%

A: Human serum albumin (5mg) was dissolved in 10mM Tris-HCl buffer of pH=7.4 to make a final concentration of 75uM.
B: Water filtered from (RO+UV+TDS controlled) purifier.
C: Synthesized using WHO protocol with reagents Isopropyl alcohol 99.8%, Hydrogen peroxide 3%, Glycerol 98%, and distilled water to make up the volume.
Table 1: Comparison of the results for Cu^{2+} detection in samples.

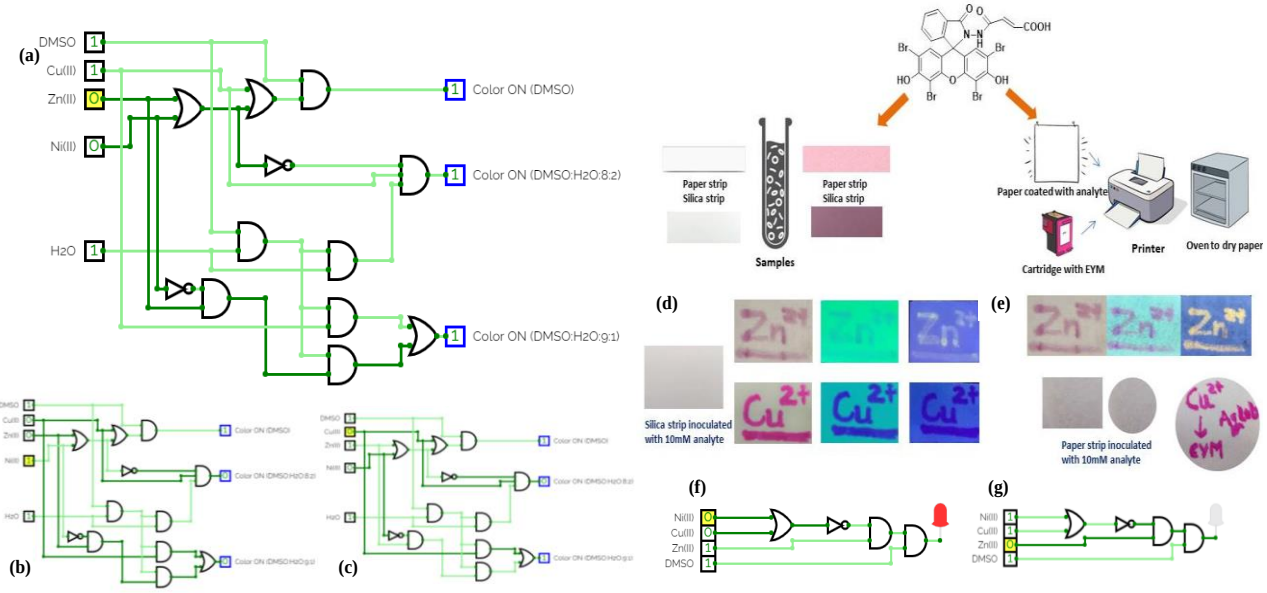

Figure 6: (a) Logic circuit for colorimetric response of **EYM** having output as color on/off in different solvent systems. Circuit display output when Cu^{2+}, DMSO, and H_2O present in system. **(b)** Logic circuit when input 1 was given for Zn^{2+}, DMSO, H_2O. **(c)** Logic circuit displays output in the presence of Ni^{2+}, DMSO, and H_2O. **(d)** Colorimetry and fluroscence response of **EYM** on analyte inoculated silica embedded strips in the presence of 1mM **EYM** and 1mM (Cu^{2+}, Zn^{2+}). **(e)** Colorimetry and fluroscence response of **EYM** on analyte inoculated whatman filter paper strips in the presence of 1mM **EYM** and 1mM (Cu^{2+}, Zn^{2+}). Inset Figures from left to right: White light image, Fluorescence image in 365nm and 254nm. **(f)** Logic circuit for colorimetric response of **EYM** having output as fluorescent-turn on in DMSO solvent system. Circuit display output a positive output for Zn^{2+} and DMSO presence in system (**g)** Logic circuit displaying a negative output when Cu^{2+} and DMSO present in system.

6. Conclusion

In summary, we successfully synthesized the novel eosin derivative **EYM** via the addition reaction between eosin hydrazide and maleic anhydride. We developed a multifunctional colorimetric, fluorescent and reversible **EYM** chemosensor that exhibited prominent absorption enhancements (at max = 540 nm) upon the addition of Cu^{2+}, with particular selectivity and sensitivity in the DMSO: H_2O (4:1 v/v %) solvent system. In addition, this sensor exhibited significant "off–on" fluorescence (at max = 559nm), accompanied by a color change from colorless to yellow fluorescence upon binding to Zn^{2+} in DMSO solvent system. Based on the coordination of **EYM**with Cu^{2+}/Zn^{2+} in a 1:2 stoichiometric ratio, we proposed ring-opening reaction mechanisms. In this study, the detection limits of the chemosensor for Cu^{2+} and Zn^{2+} is the same ~79nm. The **EYM** showed switchable selectivity and was demonstrated via UV-Vis spectroscopy where it switches between trifunctional (Cu^{2+}, Zn^{2+}, and Ni^{2+}) in DMSO solvent to bifunctional (Cu^{2+} and Zn^{2+}) in DMSO: H_2O (9:1 v/v%) solvent to monofunctional sensing for Cu2+ in DMSO: H_2O (8:2 v/v %) solvent system. In application studies, such as sensing of Cu^{2+} in practical samples, molecular encryption system, and on-time detection via paper and silica-adsorbed sensor, **EYM** exhibited considerable potential as a material to be used in the fields of biological monitoring and lab-on-a-chip tools. The proposed probe offers the advantages of a rapid, straightforward synthesis. This phenomenon enabled the real-time, simple, naked-eye detection of Cu^{2+}/Zn^{+}. We believe that **EYM** can find a potential application in chemical, biological and environmental purposes.

References

[1] J. Wang, D. Zhang, Y. Liu, P. Ding, C. Wang, Y. Ye, Y. Zhao, A N-stablization rhodamine-based fluorescent chemosensor for Fe 3+ in aqueous solution and its application in bioimaging, Sensors Actuators, B Chem. 191 (2014) 344–350.

[2] Y. Wang, H. Wu, W.N. Wu, X.J. Mao, X.L. Zhao, Z.Q. Xu, Z.H. Xu, Y.C. Fan, Novel rhodamine-based colorimetric and fluorescent sensor for the dual-channel detection of Cu 2+ and Co 2+ /trivalent metal ions and its AIRE activities, Spectrochim. Acta - Part A Mol. Biomol. Spectrosc. 212 (2019) 1–9.

[3] A. Maji, S. Lohar, S. Pal, P. Chattopadhyay, A new rhodamine based 'turn-on' Cu 2 + ion selective chemosensor in aqueous system applicable in bioimaging,

J. Chem. Sci. 129 (2017) 1423–1430. https://doi.org/10.1007/s12039-017-1349-4.

[4] C. Sun, J. Chen, H. Ma, Y. Liu, J. Zhang, Q. Liu, A new Cu2+-induced color reaction of a rhodamine derivative N-(3-carboxy)acryloyl rhodamine B hydrazide, Sci. China Chem. 54 (2011) 1101–1108.

[5] P. Puangploy, S. Smanmoo, W. Surareungchai, A new rhodamine derivative-based chemosensor for highly selective and sensitive determination of Cu2+, Sensors Actuators, B Chem. 193 (2014) 679–686. https://doi.org/10.1016/j.snb.2013.12.037.

[6] Y. Wang, H.Q. Chang, W.N. Wu, X.J. Mao, X.L. Zhao, Y. Yang, Z.Q. Xu, Z.H. Xu, L. Jia, A highly sensitive and selective colorimetric and off–on fluorescent chemosensor for Cu2+ based on rhodamine 6G hydrazide bearing thiosemicarbazide moiety, J. Photochem. Photobiol. A Chem. 335 (2017) 10–16.

[7] Y. Xiang, A. Tong, P. Jin, Y. Ju, Rhodamine Hydrazone Chemosensor for Cu (II) with High Selectivity and, Synthesis (Stuttg). (n.d.).

[8] V. Dujols, F. Ford, A.W. Czarnik, A long-wavelength fluorescent chemodosimeter selective for Cu(II) ion in water, J. Am. Chem. Soc. 119 (1997) 7386–7387. https://doi.org/10.1021/ja971221g.

[9] S. Cerutti, S. Moyano, J.A. Gásquez, J. Stripeikis, R.A. Olsina, L.D. Martinez, On-line preconcentration of cobalt in drinking water using a minicolumn packed with activated carbon coupled to electrothermal atomic absorption spectrometric determination, Spectrochim. Acta - Part B At. Spectrosc. 58 (2003) 2015–2021.

[10] S.H. Tan, G. Horlick, G. V Iyengar, W.E. Kollmer, H.J. Bowen, Determination of Trace Metals in Reference Water Standards by Inductively Coupled Plasma Mass Spectrometry with On-Line Preconcentration, Welnheim, 1989. https://pubs.acs.org/sharingguidelines.

[11] Y. Liu, P. Liang, L. Guo, Nanometer titanium dioxide immobilized on silica gel as sorbent for preconcentration of metal ions prior to their determination by inductively coupled plasma atomic emission spectrometry, Talanta. 68 (2005) 25–30.

[12] A. Lausanne, A. Kiad6, Instrumental neutron activation analysis of native copper: some methodological considerations, 1995.

[13] R.M. Roat-Malone, Copper Enzymes, in: Bioinorg. Chem., John Wiley & Sons, Inc., Hoboken, NJ, USA, 2003: pp. 187–230.

[14] R.A. Festa, D.J. Thiele, Copper: An essential metal in biology, Curr. Biol. 21 (2011) R877. https://doi.org/10.1016/j.cub.2011.09.040.

[15] Environmental Protection Agency 40 CFR Parts 141 and 142 National Primary Drinking Water Regulations for Lead and Copper: Short-Term Regulatory Revisions and Clarifications; Final Rule, 2007. www.regulations.gov (accessed April 9, 2021).

[16] E. Gaggelli, H. Kozlowski, D. Valensin, G. Valensin, Copper homeostasis and neurodegenerative disorders (Alzheimer's, prion, and Parkinson's diseases and amyotrophic lateral sclerosis), Chem. Rev. 106 (2006) 1995–2044. https://doi.org/10.1021/cr040410w.

[17] S.A. Lowndes, A.L. Harris, The role of copper in tumour angiogenesis, J. Mammary Gland Biol. Neoplasia. 10 (2005) 299–310. https://doi.org/10.1007/s10911-006-9003-7.

[18] R.A. Farrell, J.L. Thorvaldsen, D.R. Winge, Identification of the Zn(II) Site in the Copper-Responsive Yeast Transcription Factor, AMT1: A Conserved Zn Module †, 1996. https://pubs.acs.org/sharingguidelines.

[19] B. Halliwell, J.M.C. Gutteridge, Oxygen toxicity, oxygen radicals, transition metals and disease, Biochem. J. 219 (1984) 1–14. https://doi.org/10.1042/bj2190001.

[20] H. Tapiero, D.M. Townsend, K.D. Tew, Trace elements in human physiology and pathology. Copper, Biomed. Pharmacother. 57 (2003) 386–398. https://doi.org/10.1016/S0753-3322(03)00012-X.

[21] KJ Barnham, C.L. Masters, A.I. Bush, Neurodegenerative diseases and oxidatives stress, Nat. Rev. Drug Discov. 3 (2004) 205–214. https://doi.org/10.1038/nrd1330.

[22] P.G. Georgopoulos, A. Roy, M.J. Yonone-Lioy, R.E. Opiekun, P.J. Lioy, Environmental copper: Its dynamics and human exposure issues, J. Toxicol. Environ. Heal. - Part B Crit. Rev. 4 (2001) 341–394. https://doi.org/10.1080/109374001753146207.

[23] DS. Auld, Zinc Enzymes, in: Encycl. Inorg. Chem., John Wiley & Sons, Ltd, 2006. https://doi.org/10.1002/0470862106.ia259.

[24] A.I. Bush, W.H. Pettingell, G. Multhaup, M.D. Paradis, J.P. Vonsattel, J.F. Gusella, K. Beyreuther, C.L. Masters, R.E. Tanzi, Rapid induction of Alzheimer Aβ amyloid formation by zinc, Science (80-.). 265 (1994) 1464–1467. https://doi.org/10.1126/science.8073293.

[25] C.F. Walker, R.E. Black, Zinc and the risk for infectious disease, Annu. Rev. Nutr. 24 (2004) 255–275. https://doi.org/10.1146/annurev.nutr.23.011702.073054.

[26] J.Y. Koh, S.W. Suh, B.J. Gwag, Y.Y. He, C.Y. Hsu, D.W. Choi, The role of zinc in selective neuronal death after transient global cerebral ischemia, Science (80-.). 272 (1996) 1013–1016.

[27] S. Dey, A. Roy, G.P. Maiti, SK. Mandal, P. Banerjee, P. Roy, A highly selective and biocompatible chemosensor for sensitive detection of zinc(ii), New J. Chem. 40 (2016) 1365–1376. https://doi.org/10.1039/c5nj02723c.

[28] J.B. Chae, D. Yun, S. Kim, H. Lee, M. Kim, M.H. Lim, K.T. Kim, C. Kim, Fluorescent determination of zinc by a quinoline-based chemosensor in aqueous media and

zebrafish, Spectrochim. Acta - Part A Mol. Biomol. Spectrosc. 219 (2019) 74–82.
[29] Y.P. Sun, H.Y. Jung, S.H. Chang, R. Souane, S.K. Jong, S.E. Matthews, J. Vicens, A pyrenyl-appended triazole-based calix[4]arene as a fluorescent sensor for Cd2+ and Zn2+, J. Org. Chem. 73 (2008) 8212–8218.
[30] Z. Guo, G.H. Kim, J. Yoon, I. Shin, Synthesis of a highly Zn 2+-selective cyanine-based probe and its use for tracing endogenous zinc ions in cells and organisms, Nat. Protoc. 9 (2014) 1245–1254.
[31] K.S. Kasprzak, F.W. Sunderman, K. Salnikow, Nickel carcinogenesis, Mutat. Res. - Fundam. Mol. Mech. Mutagen. 533 (2003) 67–97.
[32] S.W. Ragsdale, Nickel biochemistry, Curr. Opin. Chem. Biol. 2 (1998) 208–215. https://doi.org/10.1016/S1367-5931(98)80062-8.
[33] M. Costa, Y. Yan, D. Zhao, K. Salnikow, Molecular mechanisms of nickel carcinogenesis: Gene silencing by nickel delivery to the nucleus and gene activation/inactivation by nickel-induced cell signaling, in: J. Environ. Monit., 2003: pp. 222–223. https://doi.org/10.1039/b210260a.
[34] J. Zhao, X. Shi, V. Castranova, M. Ding, Occupational toxicology of nickel and nickel compounds, J. Environ. Pathol. Toxicol. Oncol. 28 (2009) 177–208.
[35] S.W. Ragsdale, Nickel-based enzyme systems, J. Biol. Chem. 284 (2009) 18571–18575.
[36] B. Zambelli, F. Musiani, S. Benini, S. Ciurli, Chemistry of Ni2+ in urease: Sensing, trafficking, and catalysis, Acc. Chem. Res. 44 (2011) 520–530.
[37] S. Goswami, S. Chakraborty, A.K. Das, A. Manna, A. Bhattacharyya, C.K. Quah, HK Fun, Selective colorimetric and ratiometric probe for Ni(ii) in quinoxaline matrix with the single crystal X-ray structure, RSC Adv. 4 (2014) 20922–20926.
[38] A. Tamayo, J. Casabó, L. Escriche, C. Lodeiro, B. Covelo, C.D. Brondino, R. Kivekäs, R. Sillampää, Color tuning of a nickel complex with a novel N2S2 pyridine-containing macrocyclic ligand, Inorg. Chem. 45 (2006) 1140–1149.
[39] S. Chakraborty, S. Rayalu, Detection of nickel by chemo and fluoro sensing technologies, Spectrochim. Acta - Part A Mol. Biomol. Spectrosc. 245 (2021) 118915.
[40] S.C. Dodani, Q. He, C.J. Chang, A turn-on fluorescent sensor for detecting nickel in living cells, J. Am. Chem. Soc. 131 (2009) 18020–18021.
[41] D.H. Wittekind, V. Kretschmer, I. Sohmer, Azure B-eosin Y stain as the standard Romanowsky-Giemsa stain, Br. J. Haematol. 51 (1982) 391–393.
[42] Bancroft's Theory and Practice of Histological Techniques: Expert Consult ... - Kim S Suvarna, Christopher Layton, PhD, John D. Bancroft - Google Books, (n.d.).
[43] N. Klonis, W.H. Sawyer, Spectral Properties of the Prototropic Forms of Fluorescein in Aqueous Solution, 1996.
[44] PG SEYBOLD, M. GOUTERMAN, J. CALLIS, Calorimetric, photometric and lifetime determinations of fluorescence yields of fluorescein dyes, Photochem. Photobiol. 9 (1969) 229–242.
[45] M. Neumann, S. Füldner, B. König, K. Zeitler, Metal-Free, Cooperative Asymmetric Organophotoredox Catalysis with Visible Light, Angew. Chemie Int. Ed. 50 (2011) 951–954.
[46] X.-J. Yang, B. Chen, L.-Q. Zheng, L.-Z. Wu, C.-H. Tung, c3gc42042f 1082..1086 ++, 16 (2014) 1082.
[47] L. Gu, C. Jin, J. Liu, Green Chemistry COMMUNICATION Metal-free, visible-light-mediated transformation of aryl diazonium salts and (hetero)arenes: an efficient route to aryl ketones †, Green Chem. 17 (2015) 3733–3736.
[48] D. Xia, Y. Li, T. Miao, P. Li, L. Wang, Visible-light-induced dual C–C bond formation via selective C(sp3)–H bond cleavage: efficient access to alkylated oxindoles from activated alkenes and simple ethers under metal-free conditions, 19 (2017) 1732.
[49] FQ. Huang, X. Dong, L.W. Qi, B. Zhang, Visible-light photocatalytic α-amino C(sp3)–H activation through radical translocation: a novel and metal-free approach to α-alkoxybenzamides, Tetrahedron Lett. 57 (2016) 1600–1604.
[50] D. Ravelli, M. Fagnoni, A. Albini, Photoorganocatalysis. What for?, Chem. Soc. Rev. 42 (2013) 97.
[51] D. Zhao, Z. Xie, Visible-Light-Promoted Photocatalytic B−C Coupling via a Boron-Centered Carboranyl Radical: Facile Synthesis of B(3)-Arylated *o* -Carboranes, Angew. Chemie Int. Ed. 55 (2016) 3166–3170. https://doi.org/10.1002/anie.201511251.
[52] V. Srivastava, P.P. Singh, Eosin y catalysed photoredox synthesis: A review, RSC Adv. 7 (2017) 31377–31392.
[53] M. Valko, H. Morris, M. Mazúr, J. Telser, E.J.L. McInnes, F.E. Mabbs, High-affinity binding site for copper(II) in human and dog serum albumins (an EPR study), J. Phys. Chem. B. 103 (1999) 5591–5597.
[54] T. Kirsipuu, A. Zadorožnaja, J. Smirnova, M. Friedemann, T. Plitz, V. Tõugu, P. Palumaa, Copper(II)-binding equilibria in human blood, Sci. Rep. 10 (2020) 1–11.
[55] P.Z. Neumann, A. Sass-Kortsak, The state of copper in human serum: evidence for an amino acid-bound fraction., J. Clin. Invest. 46 (1967) 646–658.
[56] S. Catalani, M. Paganelli, M.E. Gilberti, L. Rozzini, F. Lanfranchi, A. Padovani, P. Apostoli, Free copper in serum: An analytical challenge and its possible applications, J. Trace Elem. Med. Biol. 45 (2018) 176–180.